LASER & PHOTONICS REVIEWS
www.lpr-journal.org

Revealing Mie Resonances with Enhanced and Suppressed Second-Order Nonlinear Optical Responses in a Hexagonal-Prism-Like MoS_2 Nanoparticle

*Mingcheng Panmai, Jin Xiang, Lidan Zhou, Shulei Li, and Sheng Lan**

Transition metal dichalcogenides (TMDC), such as molybdenum disulfide (MoS_2), have attracted great interest owing to their excellent electronic and optical properties. Efficient second harmonic generation (SHG) has been successfully demonstrated in the MoS_2 monolayer, in sharp contrast to the negligible SHG from the bulk material. Here, the nonlinear optical responses of hexagonal-prism-like MoS_2 nanoparticles are investigated, which support Mie resonances in the near infrared spectral range. It is revealed that the Mie resonances of such a MoS_2 nanoparticle can be clarified into two types, which exhibit enhanced and suppressed SHG. It is verified that the SHG from the MoS_2 nanoparticle is strongly correlated with the electric field distribution at the optical resonance. For the electric quadrupole mode with an anti-symmetric electric field distribution, the SHG is greatly suppressed. As a result, a nanohole appears in the emission pattern of the SHG from the MoS_2 nanoparticle. In sharp contrast, the SHG from the electric dipole mode with a symmetric electric field distribution can be one order of magnitude stronger than that from a MoS_2 monolayer. The findings open new horizons for manipulating the nonlinear optical responses of TMDC nanoparticles and pave the way for realizing photonic devices.

1. Introduction

Using second-order ($\chi^{(2)}$) nonlinear effect to achieve second harmonic generation (SHG) is a popular method for generating coherent light sources at extreme wavelengths. For bulk materials, the phase mismatch between the fundamental wave and the harmonic wave leads to the reduction in the conversion efficiency and various strategies have been proposed to solve this problem. In contrast, phase matching is no longer necessary for nanomaterials whose dimensions are comparable or even smaller than the wavelength of light. In this case, the enhancement of SHG relies mainly on the electric field enhancement at the wavelength of the fundamental wave. Since optical resonances in frequency domain represent the localization of electric field in spatial domain, various optical resonances have been exploited to achieve this goal, including surface plasmon resonances,[1] Mie resonances,[2] multipole resonances,[3,4] anapole mode,[5] Fabry–Perot modes,[6] whispering gallery modes,[7] epsilon-near-zero resonances,[8] and Fano resonances.[9] The state-of-the-art researches suggest that surface lattice resonances,[10] quasi-bound states in the continuum (quasi-BIC),[11–15] and supercavities[16,17] can not only realize electromagnetic field enhancement but also suppress radiation loss. The combination of these two features ultimately leads to giant SHG enhancement.

It is well known that SHG is forbidden in a centrosymmetric material with vanishing $\chi^{(2)}$ nonlinearity. This limitation can be overcome by using nanostructures. At the atomic or molecular level, the discontinuity of atoms on the surface automatically breaks the symmetry of a crystal, leading to an effective $\chi^{(2)}$ nonlinearity.[18] Alternatively, the $\chi^{(2)}$ nonlinearity can be achieved by using the nonuniformity of the electric field in the nanostructure.[19] At the macroscopic level, the $\chi^{(2)}$ nonlinearity can be obtained by using asymmetric structures.[20,21]

So far, the SHG in plasmonic nanoparticles and nanostructures have been extensively studied. Early in 2007, a multipolar tensor analysis for the SHG from a regular array of L-shaped gold nanoparticles was performed. The transmitted and reflected light of the metasurface is analyzed by dividing the tensors into symmetric (dipolar) and anti-symmetric (higher multipolar)

M. Panmai, J. Xiang, L. Zhou, S. Li, S. Lan
Guangdong Provincial Key Laboratory of Nanophotonic Functional Materials and Devices
School of Information and Optoelectronic Science and Engineering
South China Normal University
Guangzhou 510006, P. R. China
E-mail: slan@scnu.edu.cn

J. Xiang
Key Laboratory of Optoelectronic Technology and Systems (Ministry of Education)
College of Optoelectronic Engineering
Chongqing University
Chongqing 400044, P. R. China

L. Zhou
State Key Laboratory of Optoelectronic Materials and Technologies
School of Electronics and Information Technology
Sun Yat-sen University
Guangzhou 51006, P. R. China

S. Li
School of Optoelectronic Engineering
Guangdong Polytechnic Normal University
Guangzhou 510665, P. R. China

The ORCID identification number(s) for the author(s) of this article can be found under https://doi.org/10.1002/lpor.202300346

DOI: 10.1002/lpor.202300346

parts and the nonlinear response is found to be dominated by a tensor component associated with chiral symmetry breaking of the sample.[22] In addition, unidirectional nonlinear optical scattering was realized by using an array of V-shaped plasmonic antennas with symmetry breaking.[21] By using a plasmonic two-wire transmission line, it was demonstrated that the symmetry of an optical mode alone is sufficient to allow SHG even in a centrosymmetric structure made of a centrosymmetric material.[23] Significant enhancement of SHG using the Fano resonances in plasmonic heptamers of silver nanoparticles is theoretically and experimentally demonstrated. The geometry is engineered to simultaneously produce a Fano resonance at the fundamental wavelength and a higher order scattering peak at the second harmonic wavelength.[24] Surface second-order nonlinearity of metallic nanoparticles can be significantly boosted up by plasmon-induced field enhancement. However, the far-field SHG may be quenched in highly symmetric plasmonic nanostructures despite huge near-field amplification. It was demonstrated that the SHG from a single gold nanosphere is significantly enhanced when tightly coupled to a metal film. The light-induced electromagnetic asymmetry in the nanogap junction efficiently suppresses the cancellation of locally generated SHG fields. The second harmonic emission is further amplified through preferential coupling to the bright dipolar resonance mode of the nanocavity.[25]

In the last decade, the linear and nonlinear optical responses of high-index dielectric nanoparticles (e.g., Si, Ge, GaAs, and AlGaAs nanoparticles) supporting Mie resonances in the visible to near infrared spectral range have received intensive and extensive studies due to their potential applications in photonic devices. The Mie resonances of Si nanoparticles have been exploited to enhance not only the third harmonic generation (THG)[26] but also the SHG.[11] In addition, it was suggested that the directionality of the SHG emission can be manipulated by engineering the geometry and position of a GaAs nanoantenna.[27] Apart from Si nanoparticles, strong SHG was also observed in AlGaAs nanoantennas driven by both electric and magnetic resonances. The contributions of electric and magnetic nonlinear responses can be distinguished by analyzing the structure of polarization states of vector beams in the second harmonic radiation.[4] The nonlinear optical response of a dimer composed of two identical dielectric nanoparticles illuminated by a circularly polarized light was also studied. A general theory describing hybridization of multipolar modes of the coupled nanoparticles was developed to reveal nonvanishing nonlinear circular dichroism in the SHG enhanced by the multipolar resonances in the dimer. The multipolar hybridization theory was verified by the experimental results obtained for the AlGaAs dimers placed on an engineered substrate.[28]

Recently, the nonlinear optical resonances of Si nanoparticles were re-examined analytically and numerically by considering both the surface and bulk nonlinearities.[29,30] It was demonstrated that the multipolar expansion of the radiated field is dominated by dipolar and quadrupolar modes and the interference between then leads to the directivity of the nonlinear scattering.[29] After that, the surpercavity mode supported by a single subwavelength AlGaAs nanoantenna was proposed to achieve a record-high conversion efficiency, which exceeds two orders of magnitude the value observed at the Mie resonances.[16] Highly efficient SHG from a Si-based metasurface was demonstrated by exploiting the high quality (Q) factor of the quasi-BIC supported in the metasurface.[11] Very recently, it was demonstrated experimentally that an individual subwavelength dielectric resonator hosting a BIC mode can greatly boost the conversion efficiency of the SHG.[31]

It was recognized recently that transition metal dichalcogenides (TMDCs) possess high refractive indices in the visible and infrared spectral range in addition to their strong nonlinear optical responses. One can achieve highly-confined electromagnetic modes by patterning TMDCs into dielectric resonators. WS_2 disks supporting resonant optical modes were fabricated and they exhibited strong SHG enhancement in the visible light spectrum.[32] In addition, the second harmonic emission was spatially directed by using a regular array of WS_2 disks. Moreover, it was found that a metasurface composed of MoS_2 cones exhibits enhanced single-beam SHG and THG.[33] It was revealed that the interplay between the resonances of the metasurface allows for tuning of the unidirectional second harmonic wave in forward or backward direction, which is not possible in any bulk nonlinear crystal.

In this article, we investigate the nonlinear optical responses of a hexagonal-prism-like molybdenum disulfide (MoS_2) nanoparticle supporting Mie resonances in the near infrared spectral range. We characterize the Mie resonances by measuring the scattering spectrum of the MoS_2 nanoparticle and identify the electric dipole (ED) and electric quadrupole (EQ) modes based on numerical simulations. We examine the SHG at the ED and EQ resonances and correlate the enhanced and suppressed SHG with the electric field distributions in the MoS_2 nanoparticle. We obtain the emission pattern of the second harmonic radiation from the MoS_2 nanoparticle by using laser scanning confocal microscopy and identify clearly the suppressed SHG at the EQ mode. We show that the SHG at the ED mode can be one order of magnitude stronger than that from a MoS_2 monolayer.

2. Results and Discussion

In **Figure 1**a, we show schematically the structure of the MoS_2 nanoparticles studied in this work. They usually appear as hexagonal prisms, which are characterized by an edge length l and a height h. For the convenience of morphology characterization, MoS_2 nanoparticles are placed on a silica (SiO_2) substrate coated with a thin layer of indium tin oxide (ITO). In the near infrared spectrum, the refractive index of ITO is similar to that of SiO_2 and it has negligible influence on the scattering peaks of a MoS_2 nanoparticle.[31] The scanning electron microscopy (SEM) images of two typical MoS_2 nanoparticles are presented in Figure 1a (see the SEM images of more MoS_2 nanoparticles in Note S1, Supporting Information).

In Figure 1b, we present the complex permittivity of MoS_2 used in the numerical simulations reported in this work.[34] It is an anisotropic permittivity which considers the difference between the in-plane permittivity and the out-of-plane one. It is noticed that the real part of the in-plane permittivity (Re $\epsilon_{xx,}\epsilon_{yy}$) is large than 20 in the visible to near infrared spectral range. In comparison, the real part of the out-of-plane permittivity is much smaller.[35] For wavelengths longer than 750 nm, the imaginary part of the plane permittivity (Im $\epsilon_{xx,}\epsilon_{yy}$) approaches zero. It

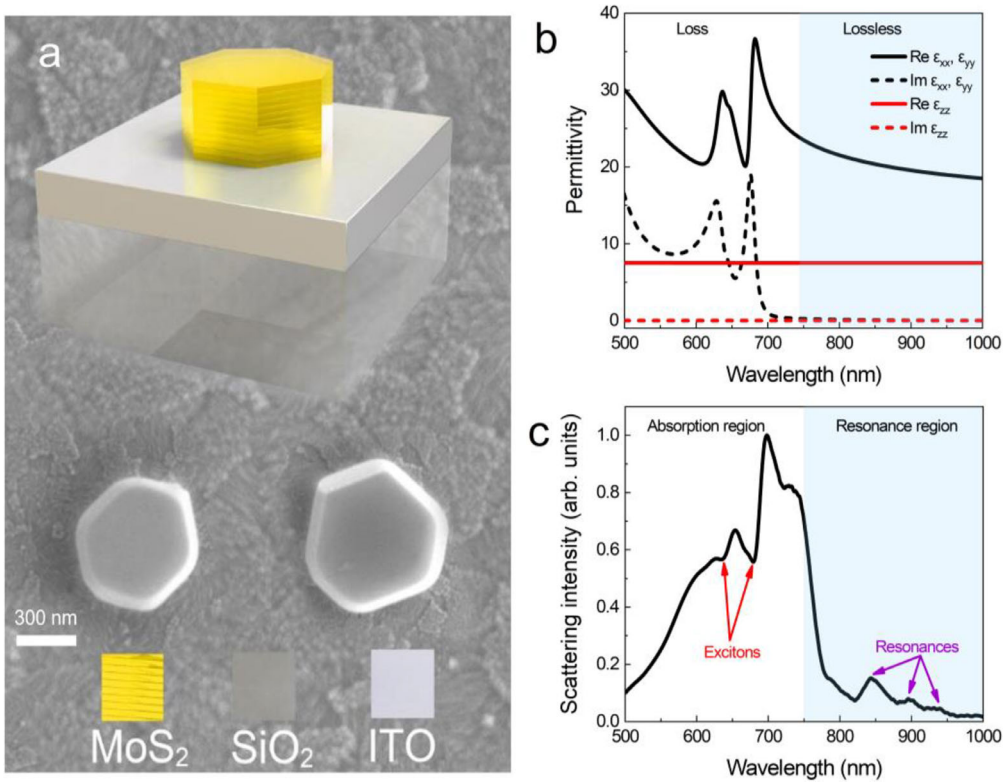

Figure 1. Structure and optical characterization of MoS_2 nanoparticles. a) Schematic showing the structure of a hexagonal-prism-like MoS_2 nanoparticle placed on an ITO/SiO_2 substrate. Also shown are the SEM images of two MoS_2 nanoparticles. b) Complex permittivity of bulk MoS_2 taken from literature. c) Scattering spectrum measured for a typical MoS_2 nanoparticle.

implies MoS_2 becomes a lossless dielectric material with a high refractive index. As a result, MoS_2 nanoparticles may support optical resonances with high Q factors in near infrared spectral range.[36–38]

In Figure 1c, we show the scattering spectrum measured for typical a MoS_2 nanoparticle in the wavelength range of 500–1000 nm. It can be divided into two regions, i.e., an absorption region and a resonance region. In the absorption region, one can identify clearly two exciton resonances, which appear as two scattering dips in the scattering spectrum. They correspond to the A- (≈615 nm) and B-exciton (≈663 nm) in MoS_2 (see more scattering spectra in Note S2, Supporting Information). It is noticed that a strong scattering peak appears at ≈700 nm in the scattering spectrum. It is caused by the largest real part of the permittivity of MoS_2 at this wavelength and the rapid decrease of the imaginary part after this wavelength. It is noticed that the intensities of the scattering peaks in the resonance region are weaker than those in the absorption region. The dramatic reduction of the real part of the permittivity is responsible for this behavior. In this work, we focus mainly on the low-order Mie resonances appearing as scattering peaks in the resonance region. Since the real part of the permittivity decreases rapid from We will inspect the SHG efficiencies at these optical resonances so that the SHG is not affected by the exciton resonances.[39–41] The high-order Mie resonances of the MoS_2 nanoparticle, which appear in the absorption region, are expected to have low Q factors.[42] This strategy allows us to analyze independently the effects of the optical resonances on the SHG of the MoS_2 nanoparticle.

In **Figure 2**a, we show the scattering spectrum measured for a MoS_2 nanoparticle in the resonance region. The SEM and atomic force microscopy (AFM) images, which are used to characterize the morphology of the MoS_2 nanoparticle, are provided in the insets. The edge length and the height of hexagonal prism are found to be $l \approx 300$ nm and $h \approx 170$ nm, respectively. One can identify two optical resonances in the scattering spectrum, which originate from the radiations of the ED mode (≈880 nm) and the EQ mode (≈810 nm) supported by the MoS_2 nanoparticle.

We simulated the scattering spectrum of the MoS_2 nanoparticle based on its structural parameters ($l = 300$ nm, $h = 170$ nm), as show in Figure 2b (see more simulation results Note S3 and S4, Supporting Information). The two optical resonances (ED and EQ modes) can be observed in the scattering spectrum. However, their wavelengths are redshifted by ≈10 nm with respect to the measured ones. In addition, the Q factors of the two modes are different in the measured and simulated scattering spectra. There are two reasons accounting for these discrepancies. One is the permittivity of MoS_2 and the other is the imperfection of the MoS_2 nanoparticle. In this work, the complex permittivity of bulk MoS_2 reported in literature is used in the numerical simulation. The actual permittivity of MoS_2 nanoparticle may be different from the reported value. In addition, it is noticed from the SEM and AFM images that the morphology of the

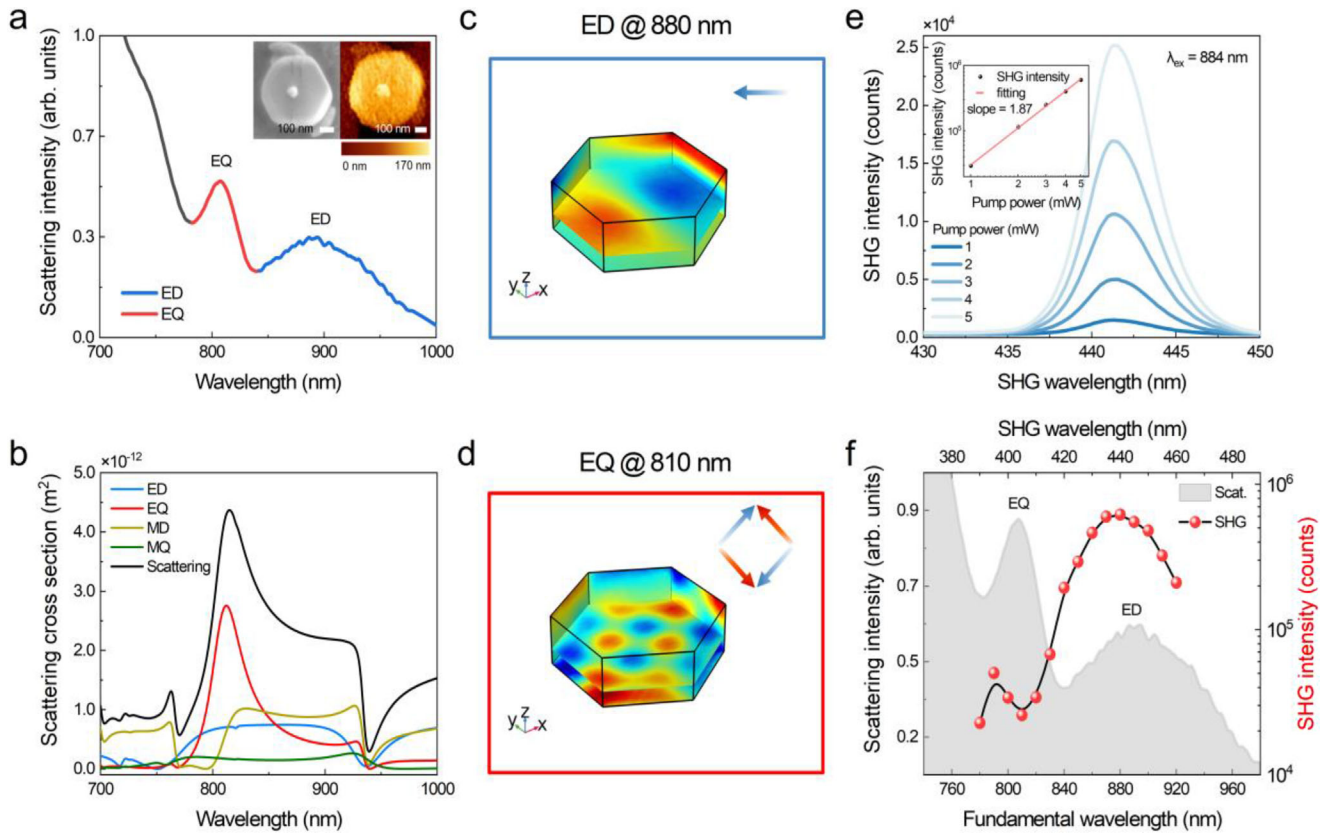

Figure 2. SHG efficiencies at different optical resonances. a) Scattering spectrum measured for a MoS_2 nanoparticle in the resonance region. The SEM and AFM images of the MoS_2 nanoparticle are shown as insets. b) Scattering spectrum simulated for a MoS_2 nanoparticle with $l = 300$ nm and $h = 170$ nm. c) Electric field distribution calculated for the ED mode of the MoS_2 nanoparticle shown in b) located at 880 nm. The arrow indicates the dipole moment. d) Electric field distribution calculated for the EQ mode the MoS_2 nanoparticle shown in b) located at 810 nm. The arrows indicate the dipole moments. e) SHG intensities measured for the MoS_2 nanoparticle shown in a) in the wavelength range of 780–920 nm. The scattering spectrum of the MoS_2 nanoparticle is provided for reference. f) SHG spectra measured for the MoS_2 nanoparticle shown in a) at an excitation wavelength of $\lambda_{ex} = 880$ nm with different pumping powers. The dependence of the SHG intensity on the pump power is presented in the inset.

MoS_2 nanoparticle deviates from a perfect hexagonal prism. In Figure 2c,d, we present the electric field distributions calculated for the ED and EQ modes located at ≈880 nm and ≈810 nm, indicating clearly the dipole moment in the ED mode and the four anti-parallel dipole moments in the EQ mode.

In Figure 2e, we show the SHG spectra obtained by resonantly exciting the ED mode with femtosecond laser pulses of different powers. The dependence of the SHG intensity on the pumping power, which is plotted in a logarithmic coordinate, is presented in the inset. A linear relationship with a slope of ≈1.87 is observed, indicating clearly the quadratic dependence of the SHG intensity on the intensity of the fundamental wave. We fixed the pumping power at $P = 5.0$ mW and examined the SHG intensities at different excitation wavelengths, as shown in Figure 2f (see Note S5, Supporting Information).

One can observe a maximum value at ≈880 nm and a minimum value at ≈810 nm, which corresponding exactly to the ED and EQ resonances in the scattering spectrum. Interestingly, the SHG intensity at the ED resonance is larger than that at the EQ resonance by a factor of ≈30. It means that the SHG of the MoS_2 nanoparticle is enhanced at the ED resonance but suppressed at the EQ resonance, although the electric field is enhanced in both cases.

For a centrosymmetric material, the gradient of electric field can be generated by an optical mode which breaks the dipole approximation at the atomic level, providing an effective bulk $\chi^{(2)}$ nonlinearity.[19] In general, a larger electric field gradient is anticipated for a high-order optical mode. Basically, one can use the fourth power of the integration of the electric field over the volume of a nanoparticle (i.e., $\int |E|^4 dV$) to characterize the SHG intensity of the nanoparticle.[20] In this regard, a high-order mode is also expected to have a larger integration of the electric field when comparing with a low-order one. However, we are surprised to find that the SHG intensity of the MoS_2 nanoparticle at the EQ resonance is much smaller than that at the ED resonance. As shown in Figure 2d, the EQ mode is composed of two paired dipole moments with equal amplitudes and opposite phases (or anti-parallel dipole moments), leading to the cancellation of the SHG in the far field due to the destructive interference of the radiations from the anti-parallel dipole moments.

The above results can be explained by comparing with the nonlinear optical responses of monolayer and multilayer MoS_2.

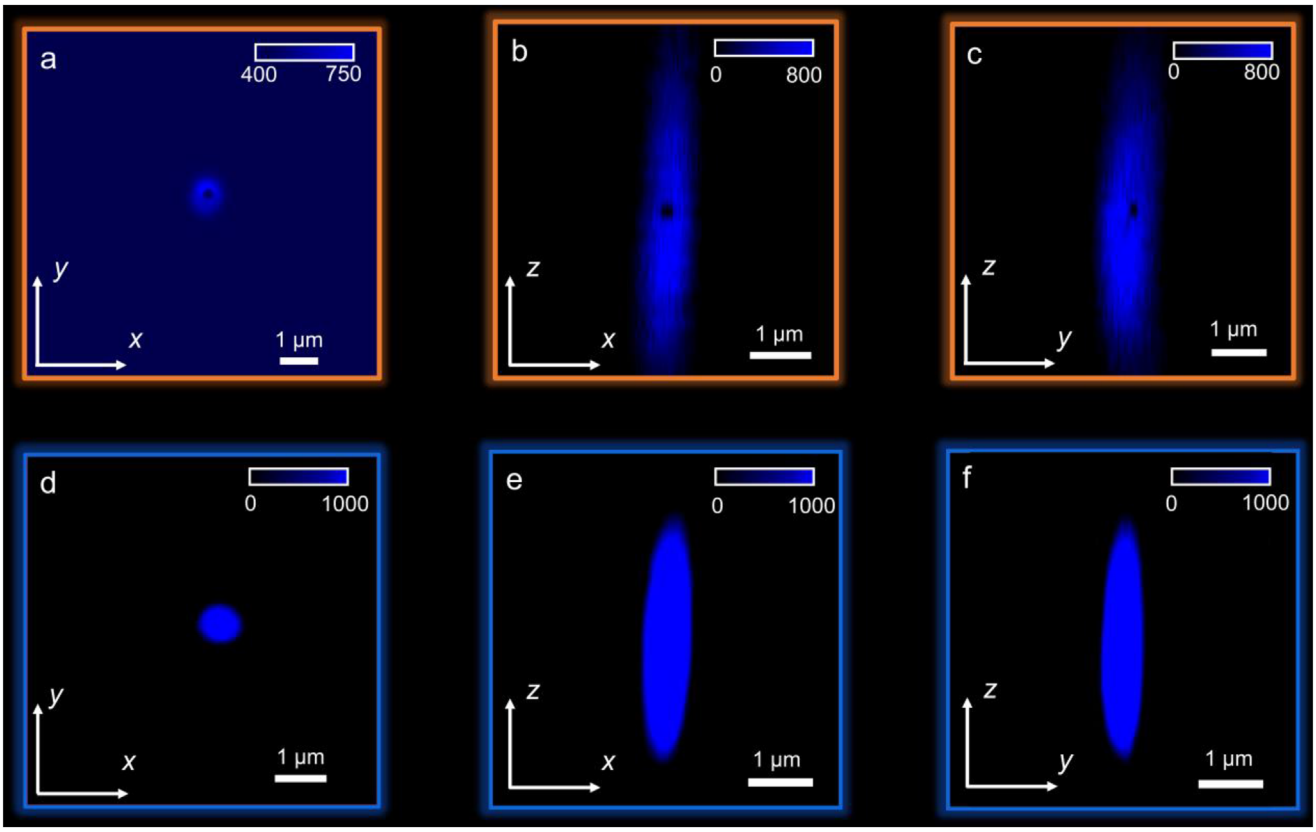

Figure 3. Emission patterns of the second harmonic wave observed at different optical resonances. a–c) 2D distributions of SHG intensity on the x–y, x–z, and y–z planes obtained for a MoS_2 nanoparticle at the EQ resonance. d–f) 2D distributions of SHG intensity on the x–y, x–z, and y–z planes obtained for a MoS_2 nanoparticle at the ED resonance. In both cases, the excitation wavelength was fixed at 800 nm.

Basically, a MoS_2 monolayer can be regarded as a horizontal dipole, providing an atomic-level $\chi^{(2)}$ nonlinearity source.[43] In comparison, there exist two $\chi^{(2)}$ nonlinearity sources with the same dipole moment but completely opposite phase in a bilayer MoS_2.[44] The interference of the radiations from these two anti-parallel dipole moments leads to the cancellation of the SHG signal in the far field.[45] For this reason, SHG is generally forbidden in a MoS_2 wafer with even layers but is allowed in that with odd layers.[46,47] This interpretation can be readily extended to the optical modes supported by a MoS_2 nanoparticle, as studied in this work. The SHG will be enhanced for optical modes with symmetric electric field distributions and suppressed for those with anti-symmetric electric field distributions. We have examined the nonlinear optical responses at the optical resonances of a few MoS_2 nanoparticles and verified the above conclusion by experimental observations (see Note S6 and S7, Supporting Information).

As discussed above, the surface and bulk nonlinearities of a MoS_2 nanoparticle contribute simultaneously to the SHG of the MoS_2 nanoparticle.[32,48] For an optical mode with an anti-symmetric electric field distribution, such as the EQ mode, the bulk nonlinearity is expected to vanish and only the surface nonlinearity is left. As a result, a suppressed SHG is anticipated at the EQ resonance.

Recently, optical far-field imaging has emerged as an powerful tool to characterize light-matter interaction and it has been successfully employed to observe self-coherent multipoles[49] and SHG.[25] In this work, we examined the SHG of a MoS_2 nanoparticle by using a confocal laser scanning microscope. In this way, the second harmonic wave emitted from the MoS_2 nanoparticle was spatially revealed by scanning the laser light across the MoS_2 nanoparticle, which is equivalent to position the MoS_2 nanoparticle at different positions of the laser beam with a Gaussian intensity distribution. The excitation wavelength was chosen at the EQ resonance of the MoS_2 nanoparticle. We examined the 3D SHG intensity of a MoS_2 nanoparticle resonantly excited at the EQ resonance (≈800 nm) (see Note S8, Supporting Information). The origin of the coordinate was chosen at the center of the MoS_2 nanoparticle. The 2D SHG intensity distributions in the x-y, y-z, and x-z planes are presented in **Figure 3**a–c, respectively. It is worth noticing that a nanohole corresponding to the disappearance of the SHG was observed when of the MoS_2 nanoparticle is located at the center of the laser beam. In addition, the size of the nanohole is comparable to that of the nanoparticle. This behavior indicates that the SHG in this case arises mainly from the surface nonlinearity and the contribution from the bulk nonlinearity is negligible. (see more scaning results in Note S9, Supporting Information). For comparison, we also inspected the 3D distribution of the SHG intensity at the ED resonance of another MoS_2 nanoparticle located at ≈800 nm (i.e., the wavelength of the femtosecond laser light) (see Note S8, Supporting Information). The corresponding 2D distributions in the x-y, y-z, and x-z planes are

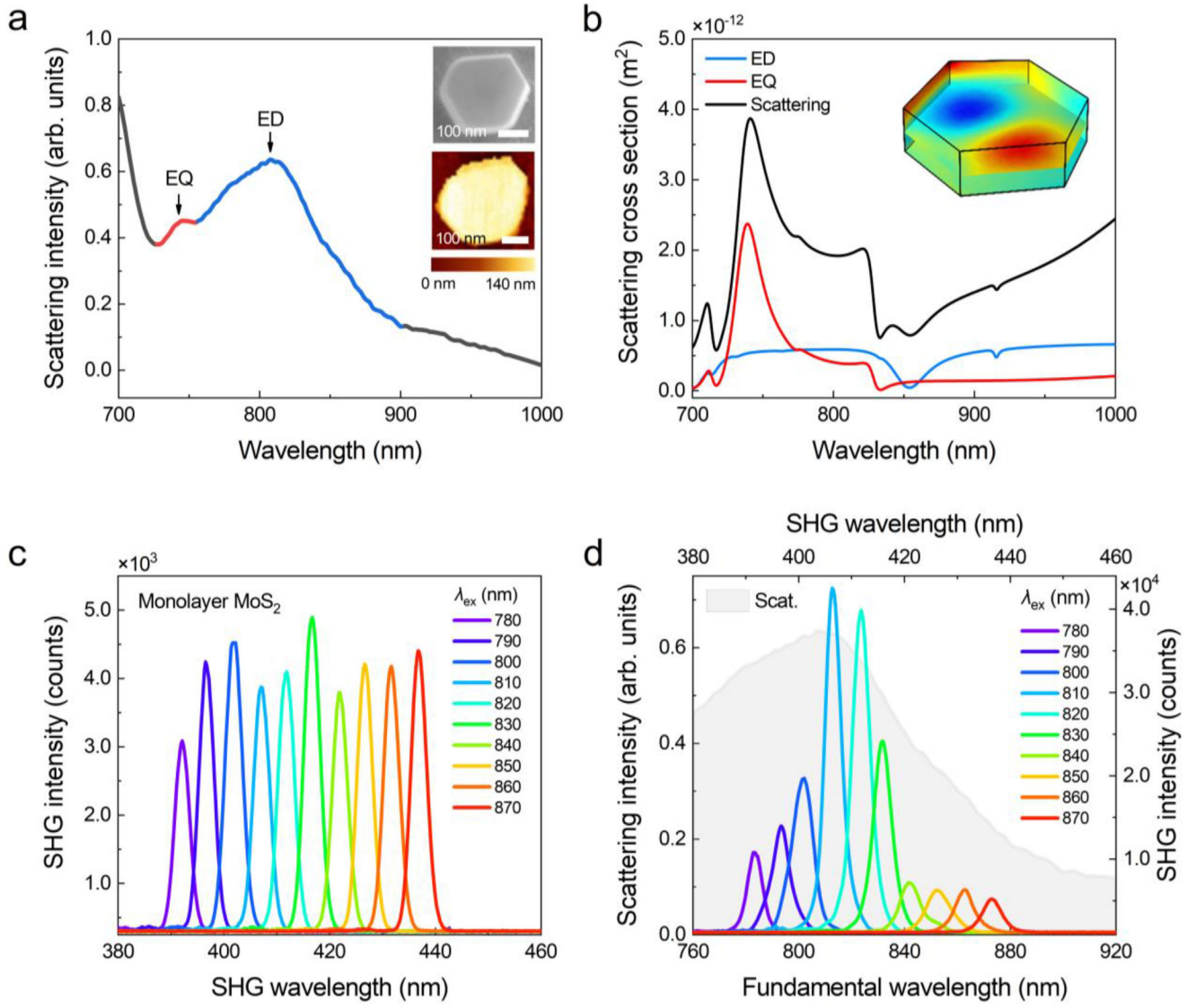

Figure 4. Enhanced SHG at the ED resonance. a) Scattering spectrum measured for a MoS_2 nanoparticle. The SEM and AFM images are shown as insets. b) Scattering spectrum simulated for the MoS_2 nanoparticle shown in (a). The electric field distribution is shown in the inset. c) SHG spectra measured for a monolayer MoS_2 at different pumping wavelengths ranging 780–870 nm. d) SHG spectra measured for a MoS_2 nanoparticle at different pumping wavelengths around the ED resonance. The scattering spectrum of the MoS_2 nanoparticle is provided for reference. In all cases, the pumping powering was fixed at $P = 5.0$ mW.

shown in Figure 3d–f. Apart from the increase in the SHG intensity, the nanohole observed previously disappeared completely.

For the ED resonance, both the surface and the bulk nonlinearity will contribute to the SHG. In this case, the SHG can be regarded as the radiation of a single dipole moment with greatly enhanced intensity. In **Figure 4**a, we show the scattering spectrum measured for a hexagonal-prism-like MoS_2 nanoparticle. The ED resonance of the MoS_2 nanoparticle appears at ≈810 nm. The SEM and AFM images of the nanoparticle are shown as insets. It can be seen that the shape of the MoS_2 nanoparticle deviates from a perfect hexagonal prism. Based on the structural parameters extracted from the morphology characterization, we calculated the scattering spectrum of the MoS_2 nanoparticle, as shown in Figure 4b. The simulated scattering spectrum is in qualitatively agreement with the measured one. The discrepancy originates mainly from the accuracy of the complex permittivity used in the numerical simulation. Based on the multipole decomposition of the scattering spectrum, it is revealed that the small scattering peak appearing on the left shoulder of the ED resonance (≈750 nm) originates from the EQ mode. In order to verify the enhancement in the SHG achieved at the ED resonance, we first examined the SHG spectra for a MoS_2 monolayer at different excitation wavelengths, as shown in Figure 4c. In this case, a MoS_2 monolayer was transferred onto the same ITO/SiO_2 substrate used to support the MoS_2 nanoparticle (see Note S10, Supporting Information). It was found that the SHG intensity is not sensitive to the excitation wavelength which was changed from 780 to 870 nm. In Figure 4d, we present the SHG spectra measured for

the MoS_2 nanoparticle at different excitation wavelengths around the ED resonance. As expected, it was found that the SHG intensity depends strongly on the excitation wavelength and the maximum SHG was observed at the ED resonance (≈810 nm). More importantly, it was found that the SHG intensity measured for the MoS_2 nanoparticle at the ED resonance was ≈8.0 times strong that that observed for the MoS_2 monolayer, which confirms undoubtedly the enhanced SHG at the ED resonance.

In order to examine the effects of Mie resonances on the SHG efficiency in MoS_2 nanoparticle with regular shapes, we also fabricated MoS_2 nanodisks from a MoS_2 film grown by chemical vapor deposition with the combination of electron beam lithography and reactive ion etching (see Note S11, Supporting Information). Unfortunately, no SHG was detected when such MoS_2 nanodisks were excited by using femtosecond laser pulses. We compared the X-ray diffraction spectra of the hexagonal-prism-like MoS_2 nanoparticles and the MoS_2 nanodisks. It was found that the hexagonal-prism-like MoS_2 nanoparticles are crystalline while the MoS_2 nanodisks are polycrystalline (see Note S11, Supporting Information). This is the reason why no SHG was observed for the MoS_2 nanodisks.

3. Conclusion

In conclusion, we have investigated the SHG of hexagonal-prism-like MoS_2 nanoparticles supporting Mie resonances in the near infrared spectral range. It was found that the SHG is enhanced at the ED resonance and suppressed at the EQ resonance. The enhanced and suppressed SHG originate from the symmetric and anti-symmetric electric field distributions in the ED and EQ modes. The disappearance of the bulk nonlinearity was clearly revealed in the radiation pattern of the SHG obtained by using a confocal laser scanning microscope. Moreover, it was found that the SHG intensity at the ED resonance is enhanced by a factor of ~8.0 as compared with that of MoS_2 monolayer. Our findings indicate the importance of the mode profile in determining the nonlinear optical responses of high-index nanoparticles and suggest the potential applications of such nanoparticles in nonlinear optical devices.

4. Experimental Section

Sample Fabrication: The MoS_2 nanoparticles and MoS_2 monolayers used in this work were purchased from Sixcarbon Tech Shenzhen. They were synthesized by using chemical vapor deposition. Hexagonal-prism-like MoS_2 nanoparticles was obtained by dispersing MoS_2 nano-powders uniformly in water and centrifuging the aqueous solution.

Optical Measurements: The linear and nonlinear optical responses of MoS_2 nanoparticles were characterized by using an inverted microscope (Observer A1, Zeiss) equipped with white light and femtosecond laser light as excitation sources.

A dark-field microscope with a home-built oblique incidence system was employed to characterize the scattering properties of MoS_2 nanoparticles. In this case, the illumination light was incident on MoS_2 nanoparticles at an angle of ≈40° and the forward scattering light was collected by the objective of the dark-field microscope.

The MoS_2 nanoparticles were excited by the femtosecond laser light focused with the 100× or 60× objective of the microscope. The SHG signals was gathered by the objective and directed to a spectrometer (SR-500i-B1, Andor) for spectral analysis or to a charge-coupled device (DU970N, Andor) for imaging. The mapping of the SHG signals from MoS_2 nanoparticles was performed by using a confocal laser scanning microscope (A1MP, Nikon).

Supporting Information

Supporting Information is available from the Wiley Online Library or from the author.

Acknowledgements

S. Lan acknowledges the financial support from the National Natural Science Foundation of China (Grant No. 12174123). S. Li acknowledges the financial support from the Natural Science Foundation of Guangdong Province, China (Grant No. 2022A1515010747).

Conflict of Interest

The authors declare no conflict of interest.

Data Availability Statement

The data that support the findings of this study are available from the corresponding author upon reasonable request.

Keywords

laser scanning confocal microscopy, Mie resonance, nanoparticles, second harmonic generation, transition metal dichalcogenides

Received: April 21, 2023
Revised: August 14, 2023
Published online:

[1] J. Butet, G. Bachelier, I. Russier-Antoine, C. Jonin, E. Benichou, P. F. Brevet, *Phys. Rev. Lett.* **2010**, *105*, 077401.
[2] F. Timpu, A. Sergeyev, N. R. Hendricks, R. Grange, *ACS Photonics* **2016**, *4*, 76.
[3] J. Butet, G. D. Bernasconi, M. Petit, A. Bouhelier, C. Yan, O. J. F. Martin, B. Cluzel, O. Demichel, *ACS Photonics* **2017**, *4*, 2923.
[4] S. S. Kruk, R. Camacho-Morales, L. Xu, M. Rahmani, D. A. Smirnova, L. Wang, H. H. Tan, C. Jagadish, D. N. Neshev, Y. S. Kivshar, *Nano Lett.* **2017**, *17*, 3914.
[5] M. Timofeeva, L. Lang, F. Timpu, C. Renaut, A. Bouravleuv, I. Shtrom, G. Cirlin, R. Grange, *Nano Lett.* **2018**, *18*, 3695.
[6] Y. Berdnikov, I. Shtrom, M. Rozhavskaya, W. Lundin, N. Hendricks, R. Grange, M. Timofeeva, *Nanotechnology* **2021**, *32*, 40LT01.
[7] M. L. Ren, W. Liu, C. O. Aspetti, L. Sun, R. Agarwal, *Nat. Commun.* **2014**, *5*, 5432.
[8] X. Wen, G. Li, C. Gu, J. Zhao, S. Wang, C. Jiang, S. Palomba, C. Martijn de Sterke, Q. Xiong, *ACS Photonics* **2018**, *5*, 2087.
[9] P. P. Vabishchevich, S. Liu, M. B. Sinclair, G. A. Keeler, G. M. Peake, I. Brener, *ACS Photonics* **2018**, *5*, 1685.
[10] D. C. Hooper, C. Kuppe, D. Wang, W. Wang, J. Guan, T. W. Odom, V. K. Valev, *Nano Lett.* **2019**, *19*, 165.
[11] Z. Liu, Y. Xu, Y. Lin, J. Xiang, T. Feng, Q. Cao, J. Li, S. Lan, J. Liu, *Phys. Rev. Lett.* **2019**, *123*, 253901.

[12] N. Bernhardt, K. Koshelev, S. J. U. White, K. W. C. Meng, J. E. Froch, S. Kim, T. T. Tran, D. Y. Choi, Y. Kivshar, A. S. Solntsev, *Nano Lett.* **2020**, *20*, 5309.
[13] A. P. Anthur, H. Zhang, R. Paniagua-Dominguez, D. A. Kalashnikov, S. T. Ha, T. W. W. Mass, A. I. Kuznetsov, L. Krivitsky, *Nano Lett.* **2020**, *20*, 8745.
[14] L. Xu, K. Zangeneh Kamali, L. Huang, M. Rahmani, A. Smirnov, R. Camacho-Morales, Y. Ma, G. Zhang, M. Woolley, D. Neshev, A. E. Miroshnichenko, *Adv. Sci. (Weinh)* **2019**, *6*, 1802119.
[15] Z. Liu, J. Wang, B. Chen, Y. Wei, W. Liu, J. Liu, *Nano Lett.* **2021**, *21*, 7405.
[16] L. Carletti, K. Koshelev, C. De Angelis, Y. Kivshar, *Phys. Rev. Lett.* **2018**, *121*, 033903.
[17] K. Koshelev, S. Kruk, E. Melik-Gaykazyan, J.-H. Choi, A. Bogdanov, H.-G. Park4, Y. Kivshar, *Science* **2020**, *367*, 288.
[18] M. Kauranen, A. V. Zayats, *Nat. Photonics* **2012**, *6*, 737.
[19] D. Smirnova, Y. S. Kivshar, *Optica* **2016**, *3*, 1241.
[20] S. Kujala, B. K. Canfield, M. Kauranen, Y. Svirko, J. Turunen, *Opt. Exp.* **2008**, *16*, 17196.
[21] H. Husu, R. Siikanen, J. Makitalo, J. Lehtolahti, J. Laukkanen, M. Kuittinen, M. Kauranen, *Nano Lett.* **2012**, *12*, 673.
[22] S. Kujala, B. K. Canfield, M. Kauranen, Y. Svirko, J. Turunen, *Phys. Rev. Lett.* **2007**, *98*, 167403.
[23] T. Y. Chen, J. Obermeier, T. Schumacher, F. C. Lin, J. S. Huang, M. Lippitz, C. B. Huang, *Nano Lett.* **2019**, *19*, 6424.
[24] K. Thyagarajan, J. Butet, O. J. Martin, *Nano Lett.* **2013**, *13*, 1847.
[25] G. C. Li, D. Lei, M. Qiu, W. Jin, S. Lan, A. V. Zayats, *Nat. Commun.* **2021**, *12*, 4326.
[26] E. V. Melik-Gaykazyan, S. S. Kruk, R. Camacho-Morales, L. Xu, M. Rahmani, K. Zangeneh Kamali, A. Lamprianidis, A. E. Miroshnichenko, A. A. Fedyanin, D. N. Neshev, Y. S. Kivshar, *ACS Photonics* **2017**, *5*, 728.
[27] G. Saerens, I. Tang, M. I. Petrov, K. Frizyuk, C. Renaut, F. Timpu, M. Reig Escalé, I. Shtrom, A. Bouravleuv, G. Cirlin, R. Grange, M. Timofeeva, *Laser Photonics Rev.* **2020**, *14*, 2000028.
[28] K. Frizyuk, E. Melik-Gaykazyan, J. H. Choi, M. I. Petrov, H. G. Park, Y. Kivshar, *Nano Lett.* **2021**, *21*, 4381.
[29] D. Smirnova, A. I. Smirnov, Y. S. Kivshar, *Phys. Rev. A* **2018**, *97*, 013807.
[30] P. R. Wiecha, A. Arbouet, C. Girard, T. Baron, V. Paillard, *Phys. Rev. B* **2016**, *93*, 125421.
[31] K. Koshelev, S. Kruk, E. Melik-Gaykazyan, J.-H. Choi, A. Bogdanov, H.-G. Park, Y. Kivshar, *Science* **2020**, *367*, 288.
[32] S. Busschaert, R. Reimann, M. Cavigelli, R. Khelifa, A. Jain, L. Novotny, *ACS Photonics* **2020**, *7*, 2482.
[33] M. Nauman, J. Yan, D. de Ceglia, M. Rahmani, K. Zangeneh Kamali, C. De Angelis, A. E. Miroshnichenko, Y. Lu, D. N. Neshev, *Nat. Commun.* **2021**, *12*, 5597.
[34] B. Munkhbat, P. Wrobel, T. J. Antosiewicz, T. O. Shegai, *ACS Photonics* **2022**, *9*, 2398.
[35] P. G. Zotev, Y. Wang, D. Andres-Penares, T. Severs-Millard, S. Randerson, X. Hu, L. Sortino, C. Louca, M. Brotons-Gisbert, T. Huq, S. Vezzoli, R. Sapienza, T. F. Krauss, B. D. Gerardot, A. I. Tartakovskii, *Laser Photonics Rev.* **2023**, *17*, 2200957.
[36] J. B. Khurgin, *ACS Photonics* **2022**, *9*, 743.
[37] A. V. Prokhorov, P. D. Terekhov, M. Y. Gubin, A. V. Shesterikov, X. Ni, V. R. Tuz, A. B. Evlyukhin, *ACS Photonics* **2022**, *9*, 3869.
[38] N. Muhammad, Y. Chen, C. W. Qiu, G. P. Wang, *Nano Lett.* **2021**, *21*, 967.
[39] C. Li, X. Lu, A. Srivastava, S. D. Storm, R. Gelfand, M. Pelton, M. Sukharev, H. Harutyunyan, *Nano Lett.* **2021**, *21*, 1599.
[40] K.-Q. Lin, S. Bange, J. M. Lupton, *Nat. Phys.* **2019**, *15*, 242.
[41] A. A. Popkova, I. M. Antropov, G. I. Tselikov, G. A. Ermolaev, I. Ozerov, R. V. Kirtaev, S. M. Novikov, A. B. Evlyukhin, A. V. Arsenin, V. O. Bessonov, V. S. Volkov, A. A. Fedyanin, *Laser Photonics Rev.* **2022**, *16*, 2100604.
[42] K. Koshelev, Y. Kivshar, *ACS Photonics* **2020**, *8*, 102.
[43] X. Yin, Z. Ye, D. A. Chenet, Y. Ye, K. O'Brien, J. C. Hone, X. Zhang, *Science* **2014**, *344*, 488.
[44] R. Ganatra, Q. Zhang, *ACS Nano* **2014**, *8*, 4074.
[45] J. Klein, J. Wierzbowski, A. Steinhoff, M. Florian, M. Rosner, F. Heimbach, K. Muller, F. Jahnke, T. O. Wehling, J. J. Finley, M. Kaniber, *Nano Lett.* **2017**, *17*, 392.
[46] L. M. Malard, T. V. Alencar, A. P. M. Barboza, K. F. Mak, A. M. de Paula, *Phys. Rev. B* **2013**, *87*, 201401(R).
[47] Y. Li, Y. Rao, K. F. Mak, Y. You, S. Wang, C. R. Dean, T. F. Heinz, *Nano Lett.* **2013**, *13*, 3329.
[48] M. Zdanowicz, S. Kujala, H. Husu, M. Kauranen, *New J. Phys.* **2011**, *13*, 023025.
[49] Y. Liu, Z. Zhou, F. Wang, G. Kewes, S. Wen, S. Burger, M. E. Wakiani, P. Xi, J. Yang, X. Yang, O. Benson, D. Jin, *Nat. Commun.* **2021**, *12*, 2019.